Received: 26 August 2025 | Revised: 9 January 2026 | Accepted: 31 March 2026 | Published online: 21 April 2026

RESEARCH ARTICLE

Journal of Optics and Photonics Research
2026, Vol. 3(3) 241–247
DOI: 10.47852/bonviewJOPR62027399

BON VIEW PUBLISHING

Comprehensive Analysis of Structural, Optical, Topographical, and Photosensing Characteristics of CuZnO Thin Films Synthesized via Facile Chemical Route

Harshal P. Borse[1], Neha P. Chaware[2], Manohar R. Patil[3], Arun V. Patil[1] and Nanasaheb P. Huse[2,*]

[1] *Department of Physics, Mahatma Gandhi Vidyamandir's Maharaja Sayajirao Gaikwad Arts, Science and Commerce College, India*

[2] *Department of Physics, Nandurbar Taluka Vidhayak Samiti's G. T. Patil Arts, Commerce and Science College, India*

[3] *Department of Chemistry, Nandurbar Taluka Vidhayak Samiti's G. T. Patil Arts, Commerce and Science College, India*

Abstract: This study outlines the low-cost synthesis of copper-doped zinc oxide (Cu:ZnO) thin films using a chemical bath deposition method performed at 50 °C. A detailed investigation of their structural, optical, and electrical properties was conducted. X-ray diffraction confirmed the successful integration of copper within the ZnO lattice, resulting in a hexagonal Wurtzite structure and an average crystallite size of 17.18 nm. The Williamson-Hall method revealed compressive strain within the films, which is expected to influence their optical and electronic behavior. UV–Vis absorption analysis showed significant light absorption in the visible spectrum, with an absorption edge close to 700 nm, indicating a band gap of approximately 2.67 eV. Topographical analysis highlighted variations in grain structure and surface roughness. Current-voltage characteristics, measured both in darkness and under 100 W light exposure, demonstrated linear behavior indicative of ohmic contact. A notable rise in photocurrent under illumination resulted in about 78.7% photosensitivity at a bias of +2 V, confirming efficient photocarrier generation.

Keywords: Cu-doped ZnO films, Wurtzite structure, Williamson-Hall analysis, surface roughness, photoresponse behavior

1. Introduction

In recent times, semiconducting materials from the II–VI group, particularly chalcogenides, have received considerable attention due to their diverse applications in optoelectronic devices. Compounds such as cadmium sulfide, cadmium telluride, and zinc oxide (ZnO) are especially promising for thin-film technologies because of their unique physical and chemical characteristics. ZnO is one of the most extensively studied n-type semiconductors, primarily due to its impressive optoelectronic behavior and a relatively wide band gap of approximately 3.37 eV [1–3]. It also possesses a high exciton binding energy (~60 meV) and crystallizes in the hexagonal wurtzite phase, attributes that enhance its suitability for various applications. ZnO nanostructures, particularly nanorods, are of great interest for use in devices such as field-effect transistors, light-emitting diodes, chemical sensors, photodetectors, and solar cells [4–9].

The functional properties of ZnO can be significantly enhanced through the incorporation of dopants. Among these, copper (Cu) is known to effectively tune the material's band gap based on its concentration within the lattice, forming a ternary Cu-doped ZnO (CuZnO) system that often exhibits reduced band gap values [10–13]. CuZnO has become a subject of growing interest due to its potential in diverse optoelectronic applications, particularly for gas sensing and solar energy harvesting [14–16]. Additionally, ZnO-based diluted magnetic semiconductors have emerged as promising candidates for spintronic technologies due to their capacity for spin-polarized laser emission, enabling developments in non-volatile memory, quantum computing, and enhanced electronic processing [17].

Copper doping not only influences the band gap but also enhances structural stability and defect density within the ZnO lattice. Several studies have shown that Cu inclusion alters internal strain and affects piezoelectric and optical properties. Lower Cu doping levels (1–3%) generally improve crystallinity, while excessive concentrations (> 5%) may lead to the formation of secondary phases [18]. To synthesize CuZnO thin films, researchers have explored various physical and chemical deposition techniques such as pulsed laser deposition (PLD) [19], electron beam

***Corresponding author:** Nanasaheb P. Huse, Department of Physics, Nandurbar Taluka Vidhayak Samiti's G. T. Patil Arts, Commerce and Science College, India. Email: drnphuse@ntvsgtpcollege.org

© The Author(s) 2026. Published by BON VIEW PUBLISHING PTE. LTD. This is an open access article under the CC BY License (https://creativecommons.org/licenses/by/4.0/).

evaporation [20], successive ionic layer adsorption and reaction (SILAR) [21], and chemical vapor deposition (CVD) [22]. Many previous studies on Cu-doped ZnO thin films rely on high-temperature or vacuum-based techniques such as sputtering, sol-gel annealing, spray pyrolysis, PLD, or CVD [23, 24]. However, among these, chemical bath deposition (CBD) has gained popularity for its simplicity, low-temperature operation, and cost-efficiency, making it suitable for large-scale production [25]. CBD is a solution-based technique widely utilized for depositing semiconductor thin films on glass substrates, primarily involving nucleation and subsequent growth of the solid phase. Key parameters such as bath temperature, reagent concentration, solution pH, and deposition duration critically influence the quality of the deposited film [26, 27].

Despite extensive research on Cu-doped ZnO thin films, few studies have systematically explored the combined effect of low-temperature CBD growth (50 °C) and controlled Cu incorporation on the optical and photosensing response. The present work demonstrates enhanced visible-light absorption and high photosensitivity achieved using a low-temperature and cost-effective CBD route, without requiring high thermal annealing or vacuum processing. Motivated by these aspects, the present investigation focuses on the fabrication of Cu-doped ZnO thin films using CBD at low temperature and for a short deposition time. This study demonstrates that high-performance Cu:ZnO photodetecting thin films can be synthesized through a very low-temperature, low-cost, and scalable solution process, achieving enhanced visible-light photosensitivity and tunable optical-electronic properties, surpassing many existing high-temperature deposition approaches.

2. Experimental Details

Glass slides made of silica were utilized as substrates for the deposition of CuZnO thin films, selected for their non-crystalline structure and low thermal expansion, which help achieve consistent film coverage. To ensure cleanliness and reproducibility, the slides underwent a cleaning process involving immersion in chromic acid at around 70 °C for 6 h, followed by thorough rinsing with laboline solution and distilled water before being left to air-dry.

For the CBD process, high-purity AR grade chemicals of Loba Chemie were used. Individual precursor solutions were prepared by dissolving 0.8 M zinc sulfate ($ZnSO_4$), 0.2 M copper sulfate ($CuSO_4$), and 0.1 M thiourea ($CS(NH_2)_2$) in 50 mL of distilled water, with continuous stirring maintaining 25% molar percentage of Cu relative to Zn only. A few drops of triethanolamine (TEA) were introduced as a complexing agent. The pH of the solution was then adjusted to approximately 11 using ammonia (NH_3), added slowly while stirring. The solution components were combined in the order of Cu, followed by Zn, and then thiourea. The mixed solution was maintained at ~50 °C in a water bath, and the cleaned slides were suspended vertically in the solution for 50 min. After deposition, the resulting films appeared uniform, well-adhered, and homogeneous having ~250 nm thickness with 5 nm/min deposition rate. After deposition, the coated substrates were vertically removed from bath and gently rinsed with distilled water to eliminate loosely adhered particles and then air dried at room temperature (~30 °C) for 30 min. A schematic illustration detailing the CBD process used for CuZnO thin-film deposition is shown in Figure 1.

3. Characterization

The deposited CuZnO thin films were analyzed for their structural, optical, and electrical characteristics. Structural evaluation was conducted using an X-ray diffractometer (BRUKER D8-Advance) employing CuKα_1 radiation (λ = 1.5406 Å), with scans performed across a 2θ range from 20° to 80°. Optical properties, including absorbance and band gap estimation, were examined using a UV-Visible spectrophotometer (PerkinElmer, LAMBDA 25) within the 400–1100 nm wavelength spectrum. Electrical behavior was assessed through current-voltage (I–V) measurements using a Keithley 2400 source meter, applying a ±2 V bias, and data were recorded under both dark conditions and illumination with a 100 W light source.

4. Results and Discussion

4.1. Structural properties

The structural features of the CuZnO thin films synthesized via chemical deposition were examined using X-ray Diffraction (XRD) across a 2θ range of 20° to 80°, as depicted in Figure 2. The XRD pattern of the Cu-doped ZnO thin film displays distinct and sharp diffraction peaks at specific 2θ angles, corresponding to clearly indexed (hkl) planes, indicating a well-crystallized structure. These peaks are consistent with Joint Committee on Powder Diffraction Standards (JCPDS) reference cards #75-0576 and #36-1451, confirming the formation of a hexagonal Wurtzite structure and successful substitution of copper within the ZnO lattice [28]. The pronounced (002) peak suggests a preferential

Figure 1
The schematic of CBD method to deposit CuZnO thin film

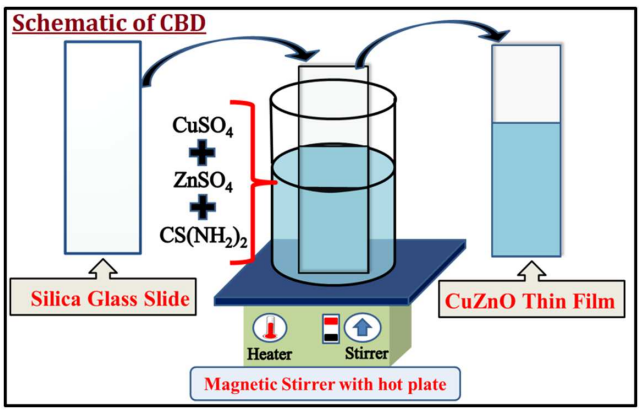

Figure 2
XRD pattern of obtained CuZnO thin film

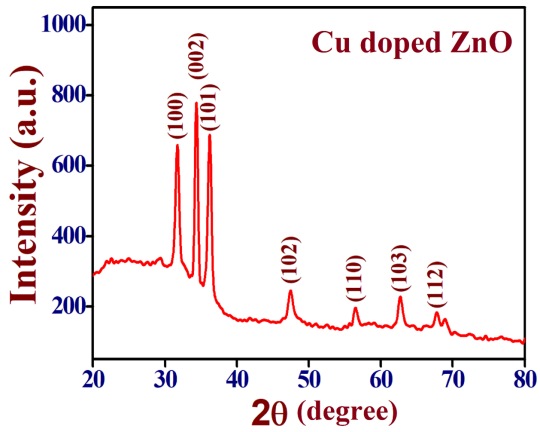

growth orientation along the c-axis, while the presence of additional reflections confirms a polycrystalline nature. A broad hump between 20° and 35° is attributed to the amorphous nature of the silica glass substrate. The slight shift in diffraction peaks toward lower 2θ values relative to undoped ZnO indicates lattice distortion, likely due to the substitution of Zn^{2+} ions (0.74 Å) with slightly smaller Cu^{2+} ions (0.73 Å). The lack of any additional peaks related to CuO or Cu_2O implies that copper is uniformly integrated without forming secondary phases. Using the Debye-Scherrer equation given in Equation (1), the average crystallite size was estimated to be around ~17.18 nm. The observed broadening of peaks suggests the presence of lattice strain and dislocation defects. Structural parameters such as dislocation density (δ) and microstrain (ε) were derived using conventional formulas given in Equations (2) and (3) [25] and are summarized in Table 1.

Figure 3(a) demonstrates the inverse relationship between crystallite size and both microstrain and dislocation density, and larger crystallites correlate with reduced internal strain and defect concentration. This trend is indicative of structural improvement during film growth, further supported by Williamson-Hall (W-H) analysis. The W-H method was applied to separate the contributions of crystallite size and lattice strain to peak broadening, as shown in Figure 3(b). In an ideal strain-free material, the plot of β cos θ against 4 sin θ would be linear and flat. However, the observed negative slope of the fitted line confirms the presence of compressive strain in the CuZnO thin film [26]. The W-H analysis reveals compressive strain within the lattice, correlated with defect and carrier modulation, an aspect rarely highlighted in earlier studies. The reduced crystallite size (~17.18 nm) contributes to enhanced surface activity and light absorption.

In the W-H plot, the x-axis (4 sin θ) reflects strain effects, and the y-axis (β cos θ) represents overall peak broadening derived from the X-ray diffraction (XRD) peaks of the sample. Despite some scatter in the data, the linear fit yields a negative slope, indicating compressive strain. In the W-H plot, the intercept provides an estimate of crystallite size which is ~26.5 nm, while the slope gives the value of strain which is approximately -1.39×10^{-4} (negative sign suggests compressive strain). These findings align with Figure 3(a), where grain growth results in strain relaxation and improved structural quality. This analysis confirms that Cu doping influences the structural characteristics of ZnO by modifying the lattice strain, which can significantly affect the optical and electrical properties of the deposited thin film.

$$D(hkl) = \frac{K\lambda}{\beta\cos\theta} \tag{1}$$

$$\delta = \frac{1}{D^2} \tag{2}$$

$$\varepsilon = \frac{\beta\cos\theta}{4} \tag{3}$$

where D is the estimated crystallite size for the (hkl) reflection, and K is a shape factor with no dimensions (0.91); β is full width at half maximum (FWHM), and λ is X-ray wavelength.

Table 1
The calculated structural factors of CuZnO thin film

2θ	(hkl) Planes	Interplanar spacing (Å)	FWHM β (10^{-3} radian)	Crystallite size D (nm)	δ (10^{14}) (lines/m^2)	$\mathcal{E}$(10^{-3})
31.64	(100)	2.819	4.41	17.072	3.4307	2.03
34.34	(002)	2.608	4.79	20.315	2.4228	1.706
36.2	(101)	2.478	4.56	17.834	3.1438	1.944
47.48	(102)	1.912	4.78	13.847	5.2151	2.503
56.51	(110)	1.626	7.21	17.406	3.3006	1.999
62.75	(103)	1.479	3.57	15.834	3.9881	2.189
67.82	(112)	1.380	4.02	18.012	3.0821	1.924
		Average values		17.18	3.3844	2.041

Figure 3
(a) The variation of dislocation density and microstrain with respect to crystallite size and (b) the W-H plot to analyze strain in the CuZnO thin film

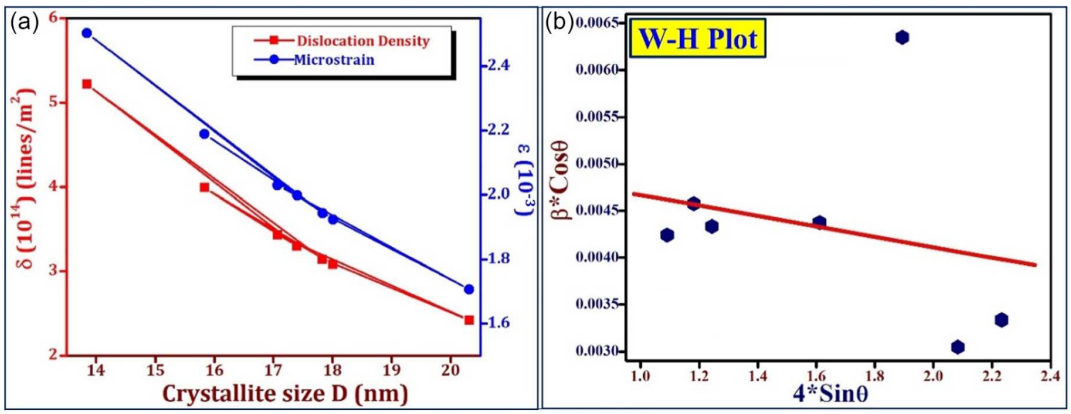

4.2. Optical properties

The optical absorbance of Cu-doped ZnO thin films was recorded at ambient temperature using a UV-Vis. spectrophotometer, covering the wavelength range from 400 to 1100 nm. As shown in Figure 4, the absorption spectrum demonstrates a gradual increase in absorbance from the visible region, with a noticeable absorption edge appearing around 700 nm, indicative of effective visible-light absorption. The strong absorption shift toward 700 nm confirms more effective utilization of visible light, superior to most reported values, making the material promising for broadband photodetectors and solar energy applications. To estimate the optical band gap, the absorbance data were processed using Tauc's method, based on the well-known Tauc relation given in Equation (4) [25, 29]. The band gap energy (E_g) was determined by extending the linear portion of the $(\alpha h\nu)^2$ versus photon energy ($h\nu$) plot to intersect the energy axis. Literature reports typically show bandgap tuning between 3.0 and 2.9 eV for Cu-doped ZnO. The resulting band gap was found to be around 2.67 eV, stating better band gap tuning with values reported in the literature. This moderately reduced band gap reflects enhanced absorption in the visible region and can be further modified by adjusting the copper doping concentration, highlighting the material's potential for applications in photoactive and optoelectronic devices.

$$\alpha = \frac{\alpha_0 \left(h\nu - E_g\right)^n}{h\nu} \tag{4}$$

According to Tauc's relation, the exponent n varies based on the type of electronic transition occurring in the material. For direct band gap semiconductors, n is equal to ½, while for indirect transitions, it takes a value of 2. In Equation (4), E_g represents the optical band gap energy, h is Planck's constant, and ν is the frequency of the incident photon.

Figure 5(a) displays a two-dimensional atomic force microscopy (AFM) image of the CuZnO thin film, where the variation in color signifies differences in surface height, reflecting nanoscale surface roughness. The scan covers a 10 µm scale, offering a broad view of surface consistency. The morphology indicates a granular texture, suggesting nanocrystalline features with non-uniform grain heights. The 3D surface profile shown in Figure 5(b) spans a region of 50 × 50 µm, with vertical height differences measured up to 980.2 nm along the z-axis. The surface exhibits a prominently textured structure with densely packed protrusions,

Figure 4
Optical absorption spectrum, with the inset illustrating the Tauc's plot of the CuZnO thin film

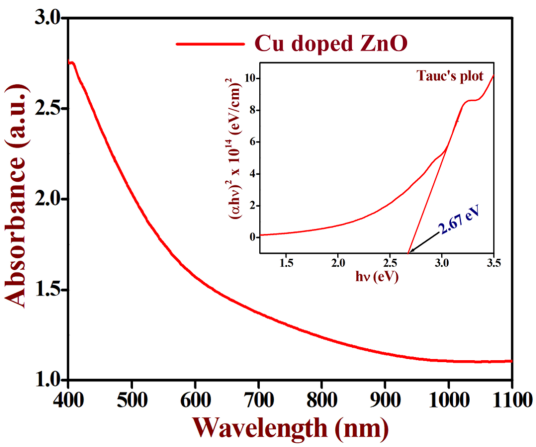

Figure 5
(a) 2D AFM image of the CuZnO thin film, (b) the corresponding 3D surface profile, and (c) a histogram analyzing the film's surface roughness

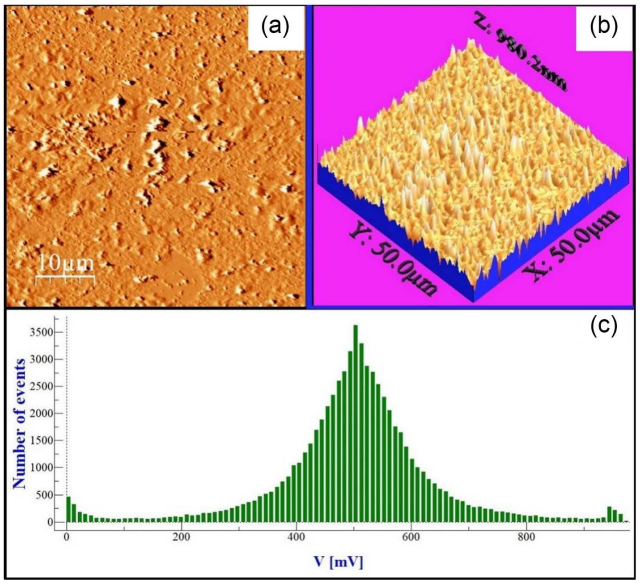

which could impact both light interaction and electrical performance. Figure 5(c) presents a histogram of the surface potential distribution across the scanned area. The x-axis (in mV) reflects the potential values, while the y-axis shows their frequency. The observed asymmetry in the distribution with a primary peak around 500 mV and secondary peaks at higher voltages suggests irregular surface potential, potentially due to non-uniform composition or surface defects. The surface roughness analysis indicates that the studied film exhibits a moderately rough surface morphology. The root mean square (RMS) roughness value is 140.85 µm and suggests the presence of noticeable height fluctuations across the scanned area. In addition, the average roughness is 94.51 µm and confirms a rough texture formed due to the grain boundaries and surface growth characteristics of the thin film.

4.3. Electrical properties

To assess the electrical performance of the CuZnO thin film, current–voltage (I-V) measurements were carried out within a bias range of ±2 V. These measurements were taken under both dark conditions and exposure to illumination from a 100-watt light AM 1.5G source, i.e., 100 mW/cm^2, covering a film area of 1×1 cm^2. Silver electrodes were applied at both ends to establish effective electrical contact. As shown in Figure 6, the I-V plots exhibit a linear trend passing through the origin, characteristic of ohmic contact typically observed at metal-semiconductor junctions. A significant rise in current under illumination indicates a clear photo response, likely due to the generation of photo-induced charge carriers. This increase in photocurrent demonstrates the film's viability for use in optoelectronic devices where light sensitivity is a crucial factor.

The photosensing capabilities of the CuZnO thin film were assessed through key parameters: photocurrent gain (P), photoresponsivity (R), and photosensitivity (S), determined using Equations (5), (6), and (7). The calculated values were 4.69%, 10.97 µA/W-cm^2, and 78.7%, respectively [3, 26]. The study demonstrates a remarkable increase in photocurrent under illumination, outperforming several reported CBD-based ZnO

Figure 6
I-V characteristics, both in the absence and presence of light of CuZnO thin film

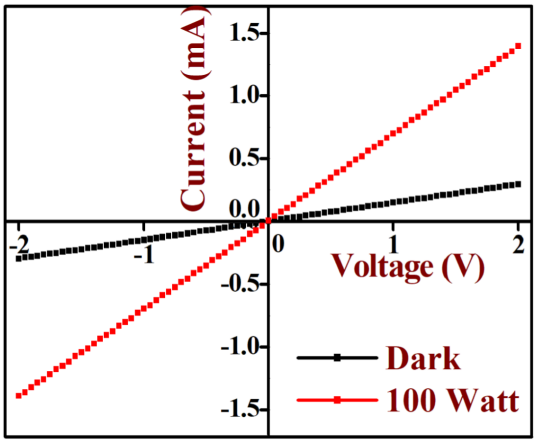

films and showing improved photo carrier generation efficiency. Linear ohmic I–V behavior indicates high-quality electrical contacts favorable for device integration. These outcomes clearly demonstrate the material's strong potential for various optoelectronic and photodetection applications, supported by its effective photo response when exposed to light.

Charge transport in Cu-doped ZnO thin films is governed by a combination of intrinsic semiconductor behavior, defect-assisted conduction, and photogenerated carrier dynamics. The incorporation of Cu ions into the ZnO lattice introduces additional acceptor-type energy states near the valence band, which enhances p-type character and facilitates charge carrier mobility. Under dark conditions, conduction primarily follows thermally activated hopping of electrons between localized defect sites such as oxygen vacancies, zinc interstitials, and Cu-related states. These defect levels act as shallow traps, enabling carriers to hop through impurity bands, resulting in a linear Ohmic I-V response as observed in the measurements. When the film is exposed to illumination, photon absorption generates a significant number of electron-hole pairs. The generated electrons move to the conduction band while holes occupy Cu-induced acceptor levels, effectively reducing recombination and increasing carrier lifetime. Additionally, photoexcitation promotes desorption of oxygen species adsorbed on the ZnO surface, which otherwise capture free electrons. This surface oxygen release increases the free carrier concentration and improves conductivity. As a result, photocurrent rises sharply compared to dark current, indicating high photosensitivity and efficient photocarrier transport.

The transport behavior under illumination can be described by a drift-diffusion mechanism, where electrons drift under the applied electric field and diffuse through grain boundaries. The moderately rough surface and grain structure support enhanced scattering paths, which contribute to carrier separation and reduced recombination probability. The observed improvement in current response under light suggests dominant mechanisms of photoexcitation, defect-mediated conduction, and trap-assisted transport.

$$P = \frac{I_p}{I_d} \tag{5}$$

$$R = \frac{I_p - I_d}{SP_i} \tag{6}$$

$$S(\%) = \frac{R_d - R_l}{R_d} \times 100 \tag{7}$$

Here, R_d represents the resistance measured in the absence of light, while R_l refers to the resistance under illumination. I_p denotes the photocurrent generated during light exposure, and I_d corresponds to the current in the dark. S stands for the active area of the thin film involved in the measurement, and P_i is the incident light power per unit area, with the total applied light intensity being 100 W.

5. Conclusion

This research thoroughly examined the photosensing characteristics of Cu-doped ZnO thin films synthesized through CBD on silica substrates. XRD analysis confirmed the development of a polycrystalline hexagonal Wurtzite structure, with no evidence of secondary copper-related phases, signifying effective Cu incorporation into the ZnO matrix. The average crystallite size was determined to be 17.18 nm, and the broadening of diffraction peaks was linked to the presence of microstrain and dislocations. A consistent reduction in both strain and defect density with increasing crystallite size highlighted the positive impact of Cu doping on the film's structural properties. W-H plots supported the presence of compressive strain, which can affect the material's optical and electronic behavior. Optical evaluation showed significant absorption in the visible range, with an optical band gap of 2.67 eV, indicating suitability for solar energy applications. AFM imaging revealed a rough, nanostructured surface that may enhance light absorption and improve device performance. Electrical measurements conducted in both dark and illuminated states demonstrated strong photosensitivity, with a notable response of approximately 78.7%, reinforcing the material's potential use in optoelectronic and photodetection systems.

Acknowledgment

The authors are thankful to the Principal of Nandurbar Taluka Vidhayak Samiti's G. T. Patil Arts, Commerce and Science College, Nandurbar, for the essential lab facilities to perform the research. We are moreover thankful to the director, IUAC, New Delhi, for characterization facilities.

Ethical Statement

This study does not contain any studies with human or animal subjects performed by any of the authors.

Conflicts of Interest

The authors declare that they have no conflicts of interest to this work.

Data Availability Statement

Data sharing is not applicable to this article as no new data were created or analyzed in this study.

Author Contribution Statement

Harshal P. Borse: Conceptualization, Methodology, Investigation, Data curation, Writing – original draft. **Neha P. Chaware:** Methodology, Software, Investigation. **Manohar R. Patil:** Writing – review & editing. **Arun V. Patil:** Writing – review & editing. **Nanasaheb P. Huse:** Conceptualization, Methodology, Software, Validation, Resources, Data curation, Writing – review & editing, Visualization, Supervision.

References

[1] Bukhtiar, A., & Zou, B. (2024). Low-dimensional II–VI semiconductor nanostructures of ternary alloys and transition metal ion doping: Synthesis, optical properties and applications. *Materials Advances*, *5*(17), 6739–6795. https://doi.org/10.1039/D4MA00523F

[2] Korotcenkov, G. (2024). II–VI semiconductor-based conductometric gas sensors: Is there a future for these sensors? *Sensors*, *24*(12), 3861. https://doi.org/10.3390/s24123861

[3] Rati, Y., Hendri, Y. N., Jonuarti, R., Marlina, R., Kurniawan, R., & Darma, Y. (2025). Visible light photodetection enhancement of co-sputtered ZnO:Cu thin films with annealing treatment. *Thin Solid Films*, *826*, 140759. https://doi.org/10.1016/j.tsf.2025.140759

[4] Bakry, M., Ismail, W., Abdelfatah, M., & El-Shaer, A. (2024). Low-cost fabrication methods of ZnO nanorods and their physical and photoelectrochemical properties for optoelectronic applications. *Scientific Reports*, *14*(1), 23788. https://doi.org/10.1038/s41598-024-73352-5

[5] Al-heuseen, K., Aljameel, A. I., & Hussein, R. K. (2024). Synthesis and characterization of Cu-Doped ZnO nanostructures for UV sensing application. *BMC Chemistry*, *18*(1), 32. https://doi.org/10.1186/s13065-024-01141-2

[6] Zhang, Y., Yang, Z., Tang, L., Shen, Y., Wu, Y., Zhang, N., . . . , & Chu, Y. (2022). UV luminescence enhancement of Cu-doped ZnO nanorods grown by hydrothermal treatment. *Journal of Luminescence*, *252*, 119364. https://doi.org/10.1016/j.jlumin.2022.119364

[7] Jayasimha, H. N., Chandrappa, K. G., Sanaulla, P. F., Dileepkumar, V. G., Nakaramontri, Y., & Pruthviraj, R. D. (2024). Synergistic effect of Cu doped ZnO nanoparticles for enhanced electrochemical sensor and photocatalytic activity. *Results in Surfaces and Interfaces*, *17*, 100351. https://doi.org/10.1016/j.rsurfi.2024.100351

[8] Lin, S., Hu, H., Zheng, W., Qu, Y., & Lai, F. (2013). Growth and optical properties of ZnO nanorod arrays on Al-doped ZnO transparent conductive film. *Nanoscale Research Letters*, *8*(1), 158. https://doi.org/10.1186/1556-276X-8-158

[9] Meena, P. L., Surela, A. K., Chhachhia, L. K., Meena, J., & Meena, R. (2025). Investigation of the photocatalytic potential of C/N-co-doped ZnO nanorods produced *via* a mechanothermal process. *Nanoscale Advances*, *7*(5), 1335–1352. https://doi.org/10.1039/D4NA00890A

[10] Sun, Y., Zhang, W., Li, Q., Liu, H., & Wang, X. (2023). Preparations and applications of zinc oxide based photocatalytic materials. *Advanced Sensor and Energy Materials*, *2*(3), 100069. https://doi.org/10.1016/j.asems.2023.100069

[11] Mohamed, K. M., Benitto, J. J., Vijaya, J. J., & Bououdina, M. (2023). Recent advances in ZnO-based nanostructures for the photocatalytic degradation of hazardous, non-biodegradable medicines. *Crystals*, *13*(2), 329. https://doi.org/10.3390/cryst13020329

[12] Rahman, M. A., Hossain, M. T., Ahmed, M. F., Bashar, M. S., Dey, S. S., Ahmed, S., & Hossain, M. S. (2025). Tuning the antimicrobial and photocatalytic activity of nano-ZnO by metal doping. *Materials Advances*, *6*(11), 3686–3704. https://doi.org/10.1039/D5MA00101C

[13] Muhammed Shafi, K., Vinodkumar, R., Bose, R. J., Uvais, V. N., & Mahadevan Pillai, V. P. (2013). Effect of Cu on the microstructure and electrical properties of Cu/ZnO thin films. *Journal of Alloys and Compounds*, *551*, 243–248. https://doi.org/10.1016/j.jallcom.2012.10.032

[14] Kamble, V. S., Zemase, R. K., Gupta, R. H., Aghav, B. D., Shaikh, S. A., Pawara, J. M., . . . , & Salunkhe, S. T. (2022). Improved toxic NO_2 gas sensing response of Cu-doped ZnO thin-film sensors derived by simple co-precipitation route. *Optical Materials*, *131*, 112706. https://doi.org/10.1016/j.optmat.2022.112706

[15] Brahma, S., Yeh, Y.-W., Huang, J.-L., & Liu, C.-P. (2021). Cu-doped p-type ZnO nanostructures as unique acetone sensor at room temperature (~25 °C). *Applied Surface Science*, *564*, 150351. https://doi.org/10.1016/j.apsusc.2021.150351

[16] Al-Mamun, M. R., Iqbal Rokon, M. Z., Rahim, M. A., Hossain, M. I., Islam, M. S., Ali, M. R., . . . , & Hossain Khan, M. Z. (2023). Enhanced photocatalytic activity of Cu and Ni-doped ZnO nanostructures: A comparative study of methyl orange dye degradation in aqueous solution. *Heliyon*, *9*(6), e16506. https://doi.org/10.1016/j.heliyon.2023.e16506

[17] Khan, R., Rasool, A., Kossar, S., Khera, E. A., Althubeiti, K., Al Otaibi, S., . . . , & Iqbal, S. (2025). Carrier-mediated ferromagnetism and dielectric tailoring in dual-doped ZnO semiconductor nanoparticles for spintronics. *Materials Science in Semiconductor Processing*, *193*, 109487. https://doi.org/10.1016/j.mssp.2025.109487

[18] Abbasi-Firouzjah, M., Shahidi, M. M., & Salahi, E. (2025). Plasma-driven growth mechanisms of ZnO:Cu sputtered Films: Emission spectroscopy insights. *Optical Materials*, *165*, 117146. https://doi.org/10.1016/j.optmat.2025.117146

[19] Singh, M., Ambedkar, A. K., Tyagi, S., Kumar, A., Kumar, A., Gautam, Y. K., . . . , & Singh, B. P. (2023). Enhanced visible-light photodetection with undoped and doped ZnO thin-film self-powered photodetectors. *ACS Omega*, *8*(40), 36966–36977. https://doi.org/10.1021/acsomega.3c04091

[20] Hasaneen, M. F., Alzaid, M., Ezzeldian, M., El-Maaref, A. A., & Hadia, N. M. A. (2025). Synthesis and physical properties of $(CdO)_{1-x}(ZnO)_x$ thin films obtained by electron beam evaporation for solar cell application. *Journal of Non-Crystalline Solids*, *660*, 123552. https://doi.org/10.1016/j.jnoncrysol.2025.123552

[21] Jellal, I., Daoudi, O., Nouneh, K., Boutamart, M., Briche, S., Plantard, G., . . . , & Naja, J. (2023). Successive ionic layer adsorption and reaction (SILAR) synthesis of micro-structured Cu-doped ZnO thin films with enhanced photocatalytic activity. *Journal of Materials Science: Materials in Electronics*, *34*(7), 672. https://doi.org/10.1007/s10854-023-10057-x

[22] Swain, B. P. (2020). The role of process temperature on structural, optical, vibrational and electronic environments of thermal chemical vapor-deposited copper-doped zinc oxide nanostructured thin films. *Applied Physics A*, *126*(8), 642. https://doi.org/10.1007/s00339-020-03824-8

[23] Sung, N.-E., Lee, I.-J., Thakur, A., Chae, K. H., Shin, H.-J., & Lee, H.-K. (2012). Properties of Cu-doped ZnO films by RF sputtering method: Thickness dependence. *Materials*

Research Bulletin, *47*(10), 2891–2894. https://doi.org/10.1016/j.materresbull.2012.04.103

[24] Chander Joshi, B., & Chaudhri, A. K. (2022). Sol–gel-derived Cu-doped ZnO thin films for optoelectronic applications. *ACS Omega*, *7*(25), 21877–21881. https://doi.org/10.1021/acsomega.2c02040

[25] Huse, N. P., Borse, H. P., Roymahapatra, G., & Sharma, R. (2024). Study of optoelectronic properties and density functional theory of kesterite Cu_2ZnSnS_4 thin film grown by facile solution growth technique. *ES Energy and Environment*, *25*, 1206. http://dx.doi.org/10.30919/esee1206

[26] Huse, N. P., Patil, R. M., & Sharma, R. (2023). Characterization of economic and non-toxic copper doped zinc sulfide thin film grown by facile chemical bath deposition method. *ES Materials and Manufacturing*, *20*, 839. http://dx.doi.org/10.30919/esmm5f839

[27] Mohammed, I. M. S., Gubari, G. M. M., Huse, N. P., Dive, A. S., Han, S.-H., & Sharma, R. (2020). Effect of Cd/S ratio on growth and physical properties of CdS thin films for photosensor application. *Journal of Materials Science: Materials in Electronics*, *31*(13), 9989–9996. https://doi.org/10.1007/s10854-020-03543-z

[28] Xu, X., Zhao, Y., Hou, H., & Liu, F. (2018). Concentration and fluid flow effects on kinetics, dendrite remelting and stress accumulation upon rapid solidification of deeply undercooled alloys. *Journal of Alloys and Compounds*, *744*, 740–749. https://doi.org/10.1016/j.jallcom.2018.02.065

[29] Devi, K. R., Selvan, G., Hari Prasad, K., Karunakaran, M., Kasirajan, K., Ganesh, V., & AlFaify, S. (2020). Effect of Cu^{2+} doping on the structural, optical, and vapor-sensing properties of ZnO thin films prepared by SILAR method. *Journal of Materials Science: Materials in Electronics*, *31*(19), 16548–16560. https://doi.org/10.1007/s10854-020-04210-z

How to Cite: Borse, H. P., Chaware, N. P., Patil, M. R., Patil, A. V., & Huse, N. P. (2026). Comprehensive Analysis of Structural, Optical, Topographical, and Photosensing Characteristics of CuZnO Thin Films Synthesized via Facile Chemical Route. *Journal of Optics and Photonics Research*, *3*(3), 241–247. https://doi.org/10.47852/bonviewJOPR62027399